Available online at www.sciencedirect.com
ScienceDirect
Journal of Sound and Vibration 298 (2006) 73–83
JOURNAL OF SOUND AND VIBRATION
www.elsevier.com/locate/jsvi

Comparison of multi-microphone transfer matrix measurements with acoustic network models of swirl burners

A. Fischer, C. Hirsch, T. Sattelmayer*

Lehrstuhl für Thermodynamik, Technische Universität München, D-85747 Garching, Germany

Received 30 April 2004; received in revised form 13 February 2006; accepted 24 April 2006
Available online 10 July 2006

Abstract

Utilizing the close analogy between electronic circuits and ducted acoustic systems, mathematical methods originally developed for the characterization of electronic networks are applied to the experimental acoustic plane wave characterization of swirl burners with complex geometries. The experiments presented in the paper show that the acoustic behavior of swirl generators can be quantitatively evaluated treating them as acoustic two-ports. Such acoustic two-ports are presented in forms of transfer-, scattering- and mobility matrices of the element. In the acoustic burner study dynamic pressure measurements were made at several locations of a tubular combustor test rig for two acoustically independent states, which were generated by forcing with sirens at the opposite ends of the setup. The technique for the experimental evaluation of acoustic transfer matrices of complex geometries on the basis of these dynamic pressure measurements is illustrated. As an alternative to the experiment, the evaluation of the acoustic behavior of acoustic systems is assessed using acoustic networks consisting of simple acoustic elements like ducts, bends, junctions and sudden area changes with transfer matrices, which are derived from first principles. In the paper, a network model representing the transfer characteristics of swirl burners is presented and compared with the previously measured transfer matrices. Although the burner geometry is rather complex, its acoustic behavior can be successfully mapped to a network consisting of a serial connection of nine elements with only minor adjustment of one parameter.

1. Introduction

For the limit of small perturbations the continuity and momentum equations can be linearized and combined to form the acoustic wave equation [1–3]. Wave equations in general describe the propagation of linear small amplitude waves in such diverse fields as acoustics, microwave engineering and optics. There are many analogies between wave propagation in electrodynamics and acoustics [4,5]. These allow the application of techniques originally developed for the mathematical description of electronic circuits to the characterization of acoustic networks. The direct transfer of the well established concept of two-ports for the representation of components in electronic network theory [6,7] results in the introduction of acoustic two-ports for the representation of acoustic components in acoustic networks [2]. In the theory of two-ports an electronic network is reduced to a black-box with an input and an output. In order to characterize the

*Corresponding author. Tel.: +49 89 289 16 210; fax: +49 89 289 16 218.

0022-460X/$ - see front matter
doi:10.1016/j.jsv.2006.04.040

black-box, at the input and output state vectors containing the state variables voltage and current are determined by experiment. The two-port is fully characterized when a linear transformation between a combination of the state variables at the input and output exists.

Depending on the combination of the state variables chosen, several representations of the acoustic two-port summarized in Table 1 exist. The specific form is selected according to practical considerations for the specific acoustic problem to be investigated. In one-dimensional plane wave acoustics pressure and velocity, which can be decomposed into the Riemann invariants $\tilde{f}$ and $\tilde{g}$ of the propagating waves, correspond to the electronic state variables voltage and current. For the experimental evaluation of the acoustic transfer characteristics the direct use of $\tilde{f}$ and $\tilde{g}$ instead of p' and u' has some advantages due to their defined direction of propagation, which allows to illustrate the influence of the investigated element on the incoming waves directly. However, from the viewpoint of combustion, the physical variables pressure p' and velocity u' are often preferred, because in particular u' in the burner throat is responsible for the modulation of the convection of the mixture and the equivalence ratio towards the flame, which governs the flame dynamics and the acoustic driving capability of the expansion due to the heat release [8]. When the electronic state variables voltage and current are replaced by their acoustic correspondents pressure p' and velocity u' or by the Riemann invariants $\tilde{f}$ and $\tilde{g}$ the concept is applicable to the characterization of acoustic black-box elements in the plane wave limit. Eq. (1) gives the definition of an acoustic transfer matrix as the linear transformation of acoustic state vectors $(p'/\bar{\rho}c, u')$over the boundaries $\mathscr{R}_u$ and $\mathscr{R}_d$ of an acoustic element (see Fig. 1).

$$\begin{pmatrix} \dfrac{p'}{\bar{\rho}c} \\ u' \end{pmatrix}_d \equiv \mathbf{T}_{pu} \cdot \begin{pmatrix} \dfrac{p'}{\bar{\rho}c} \\ u' \end{pmatrix}_u \tag{1}$$

Table 1
Acoustic two-ports in matrix form

Name	State variables	Defining equation
Transfer matrix (acoustic variables *pu*)	p', u'	$\begin{pmatrix} p'/\bar{\rho}c \\ u' \end{pmatrix}_d \equiv \mathbf{T}_{pu} \cdot \begin{pmatrix} p'/\bar{\rho}c \\ u' \end{pmatrix}_u$
Transfer matrix (Riemann invariants *fg*)	$\tilde{f}, \tilde{g}$	$\begin{pmatrix} \tilde{f} \\ \tilde{g} \end{pmatrix}_d \equiv \mathbf{T}_{fg} \cdot \begin{pmatrix} \tilde{f} \\ \tilde{g} \end{pmatrix}_u$
Scattering matrix	$\tilde{f}, \tilde{g}$	$\begin{pmatrix} \tilde{f}_d \\ \tilde{g}_u \end{pmatrix} \equiv \mathbf{S}_{fg} \cdot \begin{pmatrix} \tilde{f}_u \\ \tilde{g}_d \end{pmatrix}$
Mobility matrix	p', u'	$\begin{pmatrix} u'_u \\ u'_d \end{pmatrix} \equiv \mathbf{M}_{pu} \cdot \begin{pmatrix} p'_u/\bar{\rho}c \\ p'_d/\bar{\rho}c \end{pmatrix}$

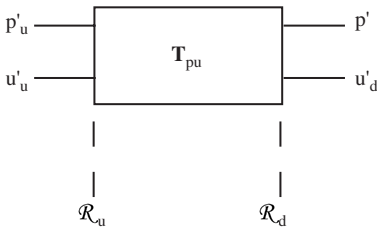

Fig. 1. The transfer matrix $\mathbf{T}_{pu}$ characterizes the transformation of the acoustic field variables pressure p' and velocity u' between the planes $\mathscr{R}_u$ and $\mathscr{R}_d$ enclosing the acoustic element.

All elements of the transfer matrix are dimensionless and of the same order of magnitude, when the factor $1/\bar{\rho}c$ is included in the definition of $\mathbf{T}_{pu}$. Eq. (1) is equivalent to the other representations of acoustic two-ports in Table 1. Each form of the acoustic two-ports can be transformed in one of the other representations. For example, the transformations from $\mathbf{T}_{pu}$ to $\mathbf{T}_{fg}$ and vice versa are

$$\mathbf{T}_{fg} = \mathbf{\Omega} \cdot \mathbf{T}_{pu} \cdot \mathbf{\Omega}^{-1},$$

$$\mathbf{T}_{pu} = \mathbf{\Omega}^{-1} \cdot \mathbf{T}_{fg} \cdot \mathbf{\Omega}, \tag{2}$$

with the transformation matrix

$$\mathbf{\Omega} = \frac{1}{2}\begin{pmatrix} 1 & 1 \\ 1 & -1 \end{pmatrix} = \frac{1}{2}\mathbf{\Omega}^{-1}. \tag{3}$$

In acoustic network modeling the acoustics of complex geometries are approximated by a network of fundamental acoustic elements. These represent the ducts, bends, junctions and changes of area constituting the geometry under investigation. Using transfer matrices the description of a successive combination of acoustic elements is straightforward. The transfer matrix $\mathbf{T}_{NW}$ of a serial network of N acoustic elements is given by the matrix product of the transfer matrices $\mathbf{T}_1 \ldots \mathbf{T}_N$ of the elements.

$$\mathbf{T}_{NW} = \mathbf{T}_N \cdot \mathbf{T}_{N-1} \cdot \ldots \cdot \mathbf{T}_1. \tag{4}$$

The acoustic analysis of complex ducted geometries is important for the design process in many fields of technical interest. In order to effectively predict and eliminate combustion driven oscillations in the development process of new combustors stability analysis tools are used [8–11] . For these tools the acoustic behavior of the acoustic elements like the transfer matrices of burner and flame are required.

2. Measurement of transfer matrices

Taking another look at Eq. (1) it becomes clear that the transfer matrix $\mathbf{T}_{pu}$ of a test element can be determined by measuring two linear independent sets of state vectors $(p'/\bar{\rho}c, u')$ in the reference planes $\mathscr{R}_u$ and $\mathscr{R}_d$ for all frequencies. The mobility matrix $\mathbf{M}_{pu}$ in Table 1 directly couples the vector (u'_u, u'_d) of the acoustic velocities in the reference planes $\mathscr{R}_u$ and $\mathscr{R}_d$ to the corresponding pressures (p'_u, p'_d). Using microphones or dynamic pressure transducers the pressure p' usually can be determined with sufficient accuracy, whereas measuring the acoustic velocity u' precisely is often difficult and requires the use of fragile hot-wire anemometers or even laser-optical equipment. Fortunately, analytic expressions for the transfer and mobility matrices $\mathbf{T}_{pu}$ and $\mathbf{M}_{pu}$ are known for many generic elements from theory [12], which allow to determine the pressures and the velocities in both reference planes from a measurement of the pressures only, if the test element is enclosed in the test at both ends by elements with known acoustic properties. Once complete state vectors (p', u') have been determined in one plane on each side, they can be propagated to any other position along the axis of element attached to the test element by application of a stepping algorithm based on the analytical solution for the wave field in tubes. As shown in Fig. 2 the measurement of acoustic transfer matrices as implemented in the *two-source location* method is based on this idea. A test element is enclosed by two regions with known mobility matrices. For simplicity, usually straight ducts are used on both sides of the test element. Pairs of microphones measure the acoustic pressures $p'_{1,a}$ to $p'_{4,a}$ and the state vectors $(p', u')_{a,u}$ and $(p', u')_{a,d}$ are calculated from the pressure data. Repeating the measurement with the acoustic source placed on the other side of the test element generates another set of linearly independent state vectors $(p', u')_{b,u}$ and $(p', u')_{b,d}$. The four elements T_{ij} of the transfer matrix $\mathbf{T}_{pu}$ are then calculated with standard numerical methods as the solution of the system of linear equations (5).

$$\begin{pmatrix} p'_a & u'_a & 0 & 0 \\ 0 & 0 & p'_a & u'_a \\ p'_b & u'_b & 0 & 0 \\ 0 & 0 & p'_b & u'_b \end{pmatrix}_u \cdot \begin{pmatrix} T_{11} \\ T_{12} \\ T_{21} \\ T_{22} \end{pmatrix} = \begin{pmatrix} p'_a \\ u'_a \\ p'_b \\ u'_b \end{pmatrix}_d . \tag{5}$$

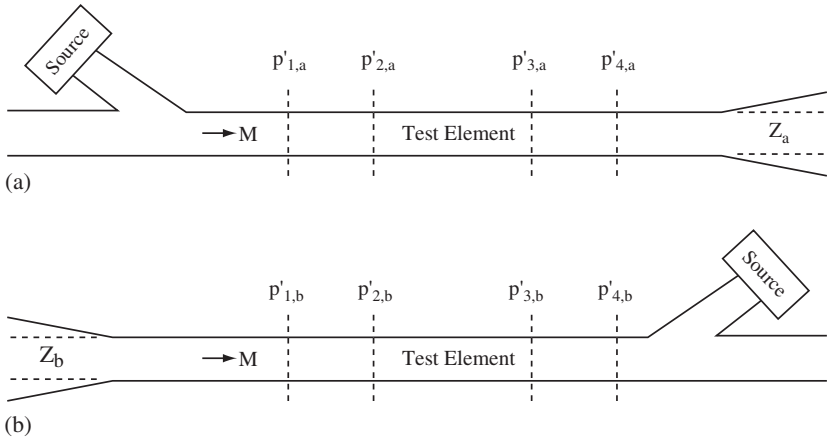

Fig. 2. Principle of the *two-source location* method (after [13]).

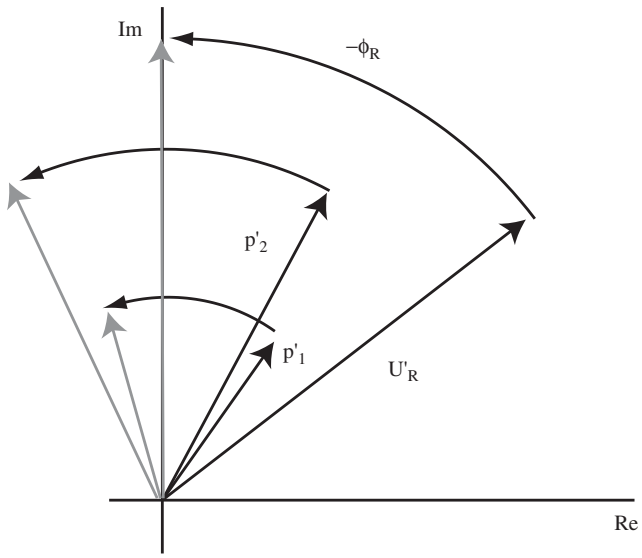

Fig. 3. Averaging of multiple measurements. The microphone pressures p'_i are rotated by the negative phase angle $-\Phi_R$ of the excitation U'_R.

Munjal and Doige demonstrated that in the *two-source location* method the excitation on different sides always delivers the required two independent states [13]. This was confirmed by experiments made by the author [12]. Åbom and Bodén discussed the method in theory [14] and various aspects of the error sensitivity of related techniques [15–18]. In order to reduce the impact of errors mainly induced by turbulent flow noise methods were developed that incorporate higher numbers of microphones on each side of the test element [19–23,12]. Monofrequent excitation is often used for the *multi-microphone method* and loudspeakers or sirens are used as acoustic sources. The multi-microphone method incorporates a nonlinear fit of the pressures at multiple ($n \geq 2$) microphone positions in order to evaluate the amplitude and phase of plane waves (Riemann invariants $\tilde{f}$ and $\tilde{g}$, Table 1) travelling in the ducts enclosing the test element. As shown by Fischer [12] nonperiodic microphone spacing is crucial to reduce the impact of singularities. These are dominant at frequencies where the distances between microphones are multiples of a half wavelength.

Over one period of the cycle all the pressure vectors at the microphone positions revolve around the origin of the complex plane. As illustrated in Fig. 3 the pressures of multiple measurements are simply averaged rotating the microphone pressures by the negative phase angle of the excitation at the acoustic source.

Incorporating trigger signals from the exciter is particularly important if sirens are used, which generate the high acoustic power required for cases with high flow noise. The trigger signal was generated using optical sensors which deliver the proper reference in cases with imperfect speed control of the siren rotor during the measurement. Introducing a larger number of microphones and averaging multiple measurements significantly increases the stability and accuracy of the method [12] particularly in cases with flow or combustion noise.

3. Experimental setup

The layout of the experimental setup is presented in Fig. 4. The burner is located downstream of a cylindrical variable length supply tube with a large number of pressure taps, which provide a flexible choice of the microphone spacing. By adjusting the length of the supply tube, the effectiveness of driving can be optimized in order to realize a suitable pulsation level in the entire frequency range investigated. On the downstream side a combustor with constant cross section, which is also equipped with pressure taps, is attached to the burner. Its length must be sufficient for the generation of a satisfactory level of dynamic pressure in the microphone section of the combustor at the lowest frequencies studied.

Albeit the test rig is designed for measurements with combustion, for the results discussed in this paper only cold flow was used. During the experiment, a constant stream of air is fed to the system. To provide a strong monofrequent excitation two sirens attached upstream or downstream of the test element, respectively, modulate the air mass flow. A bypass is integrated into the feed line to control the amplitude of the excitation by adjusting the fraction of air blown through the upstream siren. In addition, the pressure of the compressed air supplying the downstream siren is adjustable. Inside the sirens an optical detector directly records the phase and frequency of the excitation. A standard PC system equipped with a multichannel sample-and-hold board simultaneously records time series of the optic sensor signal and of eight calibrated microphones. Groups of four microphones each are arranged up- and downstream of the test element. The sensor and pressure signal time series are transformed into the frequency space with a standard Fast Fourier Transform (FFT) algorithm after applying a Hanning window. For each channel only the transformed vector corresponding to the siren excitation frequency is stored to disk for later use. Each set of vectors is rotated by the negative phase angle of the siren sensor signal (Fig. 3). After this additional step a large number of rotated pressure vectors for each frequency is averaged.

In the experiments the frequency range from 20 to 600 Hz was scanned with 20 Hz increment. For each frequency 150 independent one second time series were recorded at a sampling rate of 10 kHz. Later, from two sets of pressure data, one with upstream and one with downstream excitation, the invariant travelling wave solutions are extracted with a nonlinear Levenberg–Marquardt algorithm. From this fit, values for the

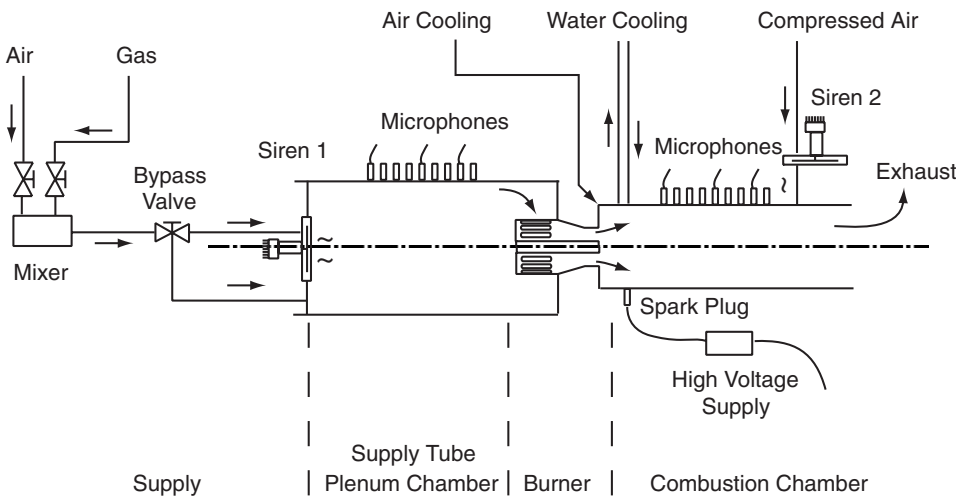

Fig. 4. Schematic sketch of the experimental setup.

Riemann invariants $\tilde{f}$ and $\tilde{g}$ at the definition planes of the test element are obtained. Solving a system of linear equations equivalent to Eq. (5) for each frequency yields the transfer matrix $\mathbf{T}_{fg}$. The transfer matrix $\mathbf{T}_{fg}$ couples vectors $(\tilde{f}, \tilde{g})$ of the Riemann invariants $\tilde{f}$ and $\tilde{g}$ at the input and output planes. The matrix $\mathbf{T}_{fg}$ is then transformed to the $\mathbf{T}_{pu}$ form with a linear matrix transformation.

4. Characterization of swirl burners

The technique described above was used for the acoustic characterization of a class of generic fully premixed swirl burners. The burner of this type ("TD[1] burner") is the central element of the test setup shown schematically in Fig. 4. During the measurements air flows through the setup at a constant flow rate of 30 g/s. As can be seen in Fig. 5 the tangential swirl generator at the burner entrance forces the stream of air into a rotating motion. The air is then accelerated in the conical nozzle before entering the combustion chamber. The swirl intensity of the burner is variable and can be increased by partial blocking of the tangential slots in the swirl generator with a modular set of disks. The burner outlet diameter can be modified using nozzle adapters with internal diameters of 32, 34, 36 and 40 mm.

Fig. 6 presents measurements of the transfer matrix for burner configurations with 36 mm nozzle exit diameter and varying swirl number (see Table 2). As in configuration 3664 the swirl generator is fully open, this case has the lowest swirl number S_{theo}. The upstream 50% of the slit are blocked in configuration 3632 and 75% in 3616. Configuration 3608 has the highest blockage and swirl number.

Interestingly, the comparison of the results reveals only small variations of the phase of the transfer matrices for different burner configurations. In contrast, the amplitudes of the elements T_{11} and T_{21} show a clear trend towards higher values for configurations with a high degree of blockage of the swirl generator. For element T_{11}, the amplitudes for configuration 3608 are, for instance, up to 75% higher than those for configuration 3664. This effect is even stronger for element T_{21}, with an increase by a factor 2.5. The gain of element T_{12} is much smaller and most likely related to an increase of the overall reduced length of the burner for a higher degree of swirl due to the increasing blockage of the flow path [25]. Finally, element T_{22} does not show any significant variations.

5. Acoustic network model

The burner shown in Fig. 5 exhibits a complicated flow path, which goes in hand with some complexity of the acoustic behavior. A successful mapping of the geometry of the TD[1] burner to a network model requires

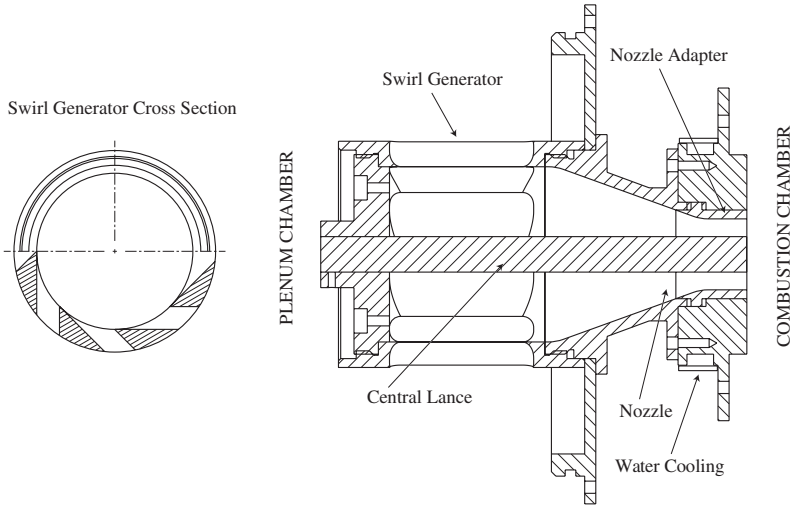

Fig. 5. Section of the TD[1] burner with 32 mm nozzle outlet diameter. The drawing on the left side illustrates the structure of the tangential swirl generator.

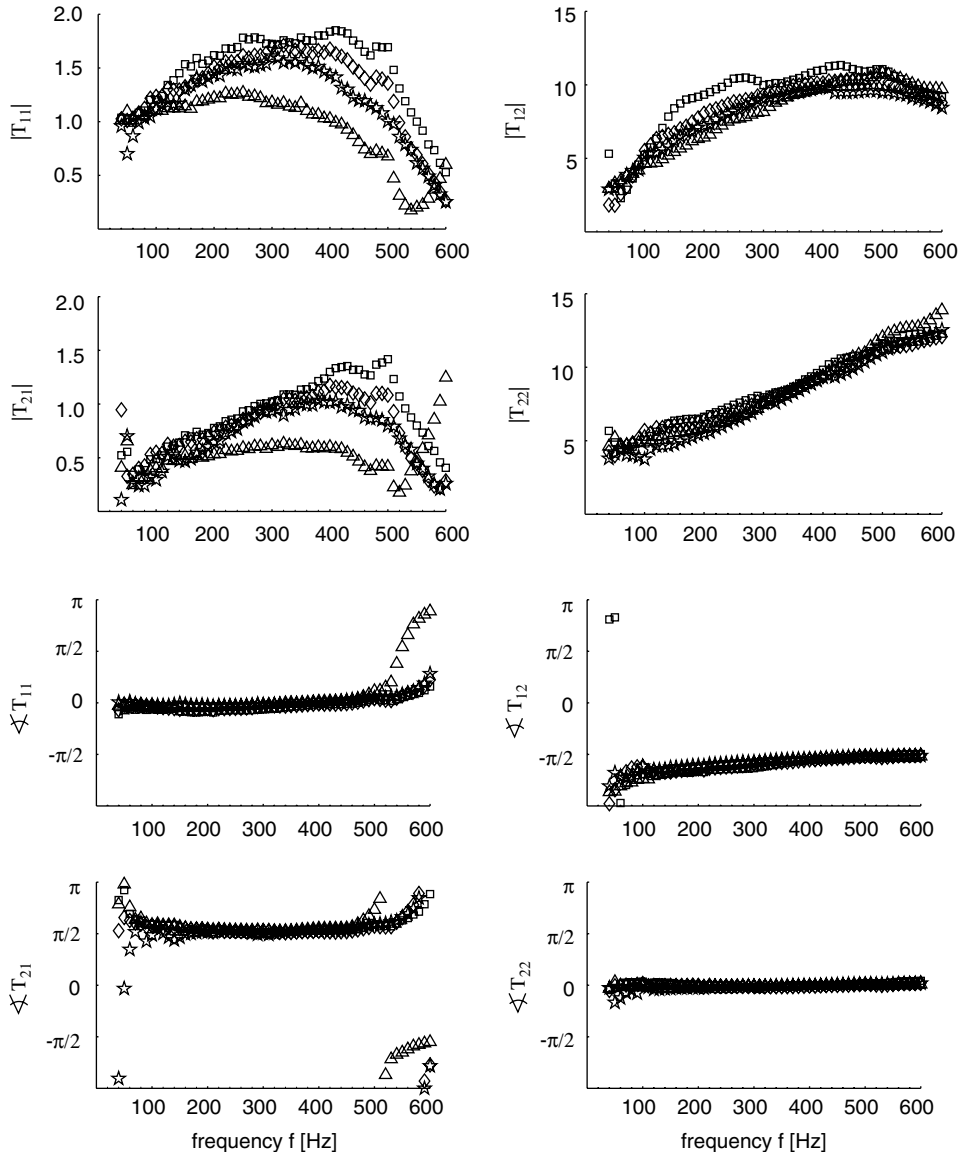

Fig. 6. Transfer matrices of the TD[1] burner for the configurations 3608 □ (highest swirl), 3616 ◇ , 3632 ⋆ and 3664 △ (lowest swirl).

Table 2
Geometric parameters and pressure loss of the TD[1] burner with a burner exit diameter of 36 mm

Configuration	Nozzle (mm)	Slit (mm)	S_{theo}	ζ_p
3664	36	64	0.26	1.12
3632	36	32	0.52	1.30
3616	36	16	1.03	1.99
3608	36	8	2.06	3.62

Swirl numbers S_{theo} are calculated from theory [24]. Pressure loss coefficients ζ_p were determined by experiment.

detailed knowledge of the critical elements. In order to improve the insight into the most important effects simpler geometries were analyzed first. Gentemann et al. presented an analytic model for the transfer matrix of sudden changes of area incorporating losses [25]. The analytic model was derived from first principles and confirmed by measurements and CFD calculations. It was shown that acoustic losses cannot be neglected whenever acoustic waves encounter sudden expansions inside a confinement. These findings were then integrated in a network model of the TD[1] burner nozzle that is in good agreement with experimental results [12]. The extension of this model to the case of the full swirl burner incorporating also the swirl generator with tangential slots of variable length will now be presented and compared with the experimental data.

Obviously, direct mapping of geometries is straightforward for simple geometries. One the other hand, validation experiments are required for systems with more complex geometry, which provide the information for some fine-tuning of the model parameters. When mapping the geometry of the TD[1] burner some essential effects have to be taken into account [12]. Consider a pressure pulse signal approaching the burner from upstream (“Plenum Chamber” in Fig. 5): When the pulse reaches the left side of the swirl generator it is partially reflected due to a change of the acoustic impedance reflecting the sudden decrease of area. When the pulse approaches the slots of the swirl generator, it is attenuated and only this attenuated wave enters the swirl generator. The other fraction of the pulse continues to propagate to the downstream end of the plenum where it is reflected. The flow field as well as the acoustic field are becoming highly three-dimensional at the burner entrance so that the approximation of plane wave acoustics does not hold in this region. In a network model this has to be considered by introduction of an extra acoustic length. When the pulse finally enters the nozzle it approaches a region with a continuous change of impedance which can be modeled by a cascade of duct segments and area changes in the acoustic network model. The continuous change of impedance inside the nozzle results in a broadening of the incoming pulse [26,27]. Most important is the massive expansion at the burner exit introducing significant acoustic losses that are considered in the analytic model of the sudden area change and do not require experimental data. However, an accurate prediction of the influence of flow losses, which also lead to acoustic losses is essential in the framework of the stability calculation of combustion systems.

Consideration of these effects leads to the acoustic network model of the TD[1] burner. It consists of the following elements (see also Figs. 4 and 5 for illustration) arranged sequentially in streamwise direction:

(1) Area change without losses. This element represents the transition from the supply tube to the partially blocked section forming an annulus with the swirl generator in the center.
(2) Duct segment of 116 mm length. This element has been selected a little longer than the physical length of 111 mm in order to account for the three-dimensional structure of the flow field near the swirl generator.
(3) Area change without losses, which represents the change of the open area between the partially blocked section forming an annulus and the inlet plane of the nozzle.
(4) Pressure loss element considering pressure losses over the burner. The experimentally determined pressure loss coefficients ζ_p from Table 2 are used in the calculations.
(5) Discrete model of the burner nozzle consisting of five duct segments joined by isentropic area changes with a total length of 52 mm.
(6) Duct segment of 30 mm length.
(7) Compact element with acoustic losses due to the sudden area change, modeling the transition from the burner exit and the combustion chamber.
(8) Finally two duct elements with 111 and −68 mm length are added. These are introduced in the network model for the purpose of shifting the reference planes $\mathscr{R}_u = \mathscr{R}_d$ to one common position. Since the burner becomes formally an element with zero length to be placed at the combustor front panel, this allows a simple use of the burner model in complex acoustic combustor networks.

The analytical form of the nine acoustic elements is summarized in Table 3. With the exception of the element 2 all other elements are fully defined on the basis of geometrical data of the burner and fluid properties and do not require any input from experiments. Element 4 requires the static pressure loss coefficient of the swirler, which is already known in most cases from pressure loss measurements. Although the model performs satisfactorily on this basis, further improvements are achieved, if a length of 116 mm is used in the model for

Table 3
Transfer matrices for the modeling of swirl burners with acoustic network models

Straight duct	$\begin{pmatrix} \cos kl & \mathrm{i}\sin kl \\ \mathrm{i}\sin kl & \cos kl \end{pmatrix}$
Area change	$\begin{pmatrix} 1 & 0 \\ 0 & A_d/A_u \end{pmatrix}$
Compact element with loss	$\begin{pmatrix} 1 & \left[1-\zeta-\left(\frac{A_u}{A_d}\right)^2\right]M_u - \mathrm{i}\frac{\omega}{c}l_{\mathrm{eff}} \\ -\mathrm{i}\frac{\omega}{c}l_{\mathrm{red}} - M_d & \frac{A_u}{A_d} \end{pmatrix}$
	$\zeta = \frac{R_a A_u}{\bar{\rho}c} \quad d_v = \sqrt{\frac{2\mu}{\bar{\rho}\omega}}$
	$l_{\mathrm{eff}} = \frac{L_a A_u}{\bar{\rho}} \quad l_{\mathrm{red}} = -\frac{\bar{\rho}}{L_a c}$
Analogous resistance	$R_a = \frac{\bar{\rho}\omega d_v \lvert D_d - D_u\rvert}{2D_d z \quad D_u}\left(1 + \frac{\lvert D_d^2 - D_u^2\rvert}{\pi D_d D_u}\ln\frac{D_d + D_u}{\lvert D_d - D_u\rvert}\right)$
Analogous inductance	$L_a = \frac{\bar{\rho}}{\pi z}\left[\frac{(D_d - D_u)^2}{2D_d D_u}\ln\frac{D_d + D_u}{\lvert D_d - D_u\rvert} + \ln\frac{(D_d + D_u)^2}{4D_d D_u}\right]$
Pressure loss	$\begin{pmatrix} 1 & -\zeta_p M\sqrt{\frac{\omega D_{\mathrm{hyd}}}{c}} \\ 0 & 1 \end{pmatrix}$

A_u, upstream cross sectional area; A_d, downstream cross sectional area; D_{hyd}, hydraulic diameter; D_u, upstream diameter; D_d, downstream diameter; l, length of duct; l_{eff}, effective length; l_{red}, reduced length; M, Mach number; ζ, acoustic loss coefficient; ζ_p, pressure loss coefficient.

element 4, although the geometrical length is 111 mm only. Fig. 7 shows a comparison of experimental results for the burner configurations 3616 and 3664 with the prediction from the acoustic network model after the minor tuning of this one model parameter was incorporated. The quality of the model is remarkable, as the model predicts the amplitudes as well as the phases of all elements of the transfer matrices with high precision.

6. Summary

The transfer matrices of geometrically complex swirl burners were measured with a multi-microphone method.

In cases with high flow noise, the acquisition of high quality data is demanding. Sufficient precision can be achieved using the high acoustic input of sirens of a special design with a low content of harmonics. For the suppression of the stochastic flow noise a large number of measurements are required for each frequency. Proper averaging requires a proper reference signal from optical sensors integrated into the acoustic driver.

A comparison of the results for different burner configurations showed no impact of the swirl number on the phase and a clear trend towards increasing amplitudes with swirl.

The results of the acoustic network model obtained after a mapping of the burner geometry are in excellent agreement with the measurements, revealing that the combined approach of low-order modeling with minor parameter optimization on the basis of experiments leads to precise one-dimensional models for elements with complicated geometries.

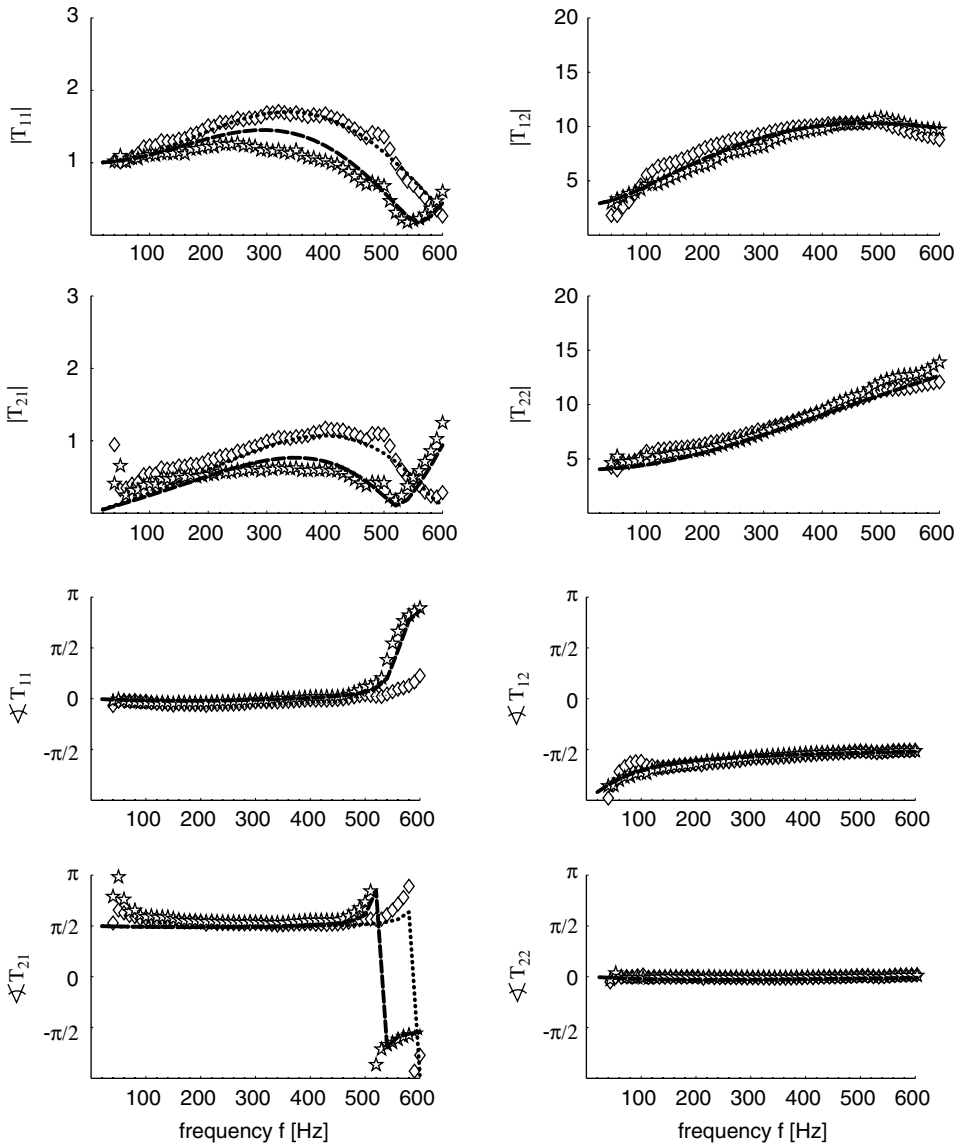

Fig. 7. Transfer matrix of the TD[1] burner: experimental results and acoustic network model calculations for the geometries 3616 (◇ measurement and ··· network model) and 3664 (⋆ measurement and —— network model).

Acknowledgments

The support of the German Bundesministerium für Bildung und Forschung and of Siemens Power Generation is gratefully acknowledged.

References

[1] P.M. Morse, K.U. Ingard, *Theoretical Acoustics*, Princeton University Press, Princeton, NJ, 1986.
[2] A.D. Pierce, *Acoustics—An Introduction to its Physical Principles and Applications*, McGraw-Hill, Boston, 1981.
[3] A.P. Dowling, J.E. Ffowces Williams, *Sound and Sources of Sound*, Ellis Horwood Limited, Chichester, West Sussex, UK, 1983.
[4] H.F. Olson, *Dynamical Analogies*, Van Nostrand, Princeton, NJ, 1958.
[5] A. Lenk, *Elektromechanische Syteme—mechanische und akustische Netzwerke, deren Wechselwirkungen und Anwendungen*, Springer, Berlin, 2001.

[6] N. Balabian, T. Bickart, *Electric Network Theory*, Wiley, New York, 1969.
[7] F. Benson, T. Benson (Eds.), *Fields Waves and Transmission Lines*, first ed., Chapman & Hall, London, 1991.
[8] T. Sattelmayer, Influence of the combustor aerodynamics on combustion instabilities from equivalence ratio fluctuations, *Journal of Engineering of Gas Turbines and Power* 125 (2003) 11–19.
[9] W. Polifke, C. Paschereit, T. Sattelmayer, *A universally applicable stability criterion for complex thermoacoustic systems*, 18. Deutsch-Niederländischer Flammentag, Delft, NL, 1997 (1997) 455–460.
[10] T. Sattelmayer, W. Polifke, Assessments of methods for the computation of the linear stability of combustors, *Combustion Science and Technology* 175 (3) (2003) 453–476.
[11] T. Sattelmayer, W. Polifke, A novel method for the computation of the linear stability of combustors, *Combustion Science and Technology* 175 (3) (2003) 477–497.
[12] A. Fischer, Hybride, thermoakustische Charakterisierung von Drallbrennern, PhD Thesis, Technische Universität München, 2004.
[13] M. Munjal, A. Doige, Theory of a two source-location method for direct experimental evaluation of the four-pole parameters of an aeroacoustic element, *Journal of Sound and Vibration* 141 (2) (1990) 323–333.
[14] M. Åbom, A note on the experimental determination of acoustical two-port matrices, *Journal of Sound and Vibration* 155 (1) (1992) 185–188.
[15] M. Åbom, A note on random errors in frequency response estimators, *Journal of Sound and Vibration* 107 (2) (1986) 355–358.
[16] H. Bodén, M. Åbom, Influence of errors on the two-microphone method for measuring acoustic properties in ducts, *Journal of the Acoustical Society of America* 79 (2) (1986) 541–549.
[17] M. Åbom, H. Bodén, Error analysis of two-microphone measurements in ducts with flow, *Journal of the Acoustical Society of America* 83 (6) (1988) 2429–2438.
[18] M. Åbom, Measurement of the scattering-matrix of acoustical two-ports, *Mechanical Systems and Signal Processing* 5 (1991) 89–104.
[19] D. Ronneberger, C. Ahrens, Wall shear stress caused by small amplitude perturbations of turbulent boundary layer flow: an experimental investigation, *Journal of Fluid Mechanics* 83 (3) (1977) 433–464.
[20] M. Peters, Aeroacoustic Sources in Internal Flow, PhD Thesis, Technische Universiteit Eindhoven, Eindhoven, NL, 1993.
[21] M. Peters, A. Hirschberg, A. Reijnen, A. Wijnands, Damping and reflection coefficient measurement for an open pipe at low mach and helmholtz numbers, *Journal of Fluid Mechanics* 256 (1993) 499–534.
[22] C. Paschereit, B. Schuermans, W. Polifke, O. Mattson, Measurement of transfer matrices and source terms of premixed flames, *Proceedings of the IGTI 1999 ASME TURBO EXPO*, Indianapolis, Indiana, USA paper 99-GT-133.
[23] B. Schuermans, Modeling and Control of Thermoacoustic Instabilities, PhD Thesis, École Polytechnique Fédérale de Lausanne (EPFL), 2003.
[24] C. Schmid, Drallbrennersimulation durch Starrkörperwirbelströmungen unter Einbeziehung von drallfreier Primärluft und Verbrennung, PhD Thesis, Universität Karlsruhe, 1991.
[25] A. Gentemann, A. Fischer, S. Evesque, W. Polifke, Acoustic transfer matrix reconstruction and analysis for ducts with sudden change of area, *Ninth AIAA/CEAS Aeroacoustics Conference and Exhibit*, Hilton Head.
[26] D.P. Berners, Acoustics and Signal Processing Techniques for Physical Modelling of Brass Instruments, PhD Thesis, Stanford University, 1999.
[27] D.P. Berners, Acoustics and Signal Processing Techniques for Physical Modelling of Brass Instruments, http://ccrma-www.stanford.edu/~dpberner/Defense/pres.html, Thesis defence presentation, April 1999.